Journal of Materials Chemistry

Cite this: J. Mater. Chem., 2011, 21, 8038

www.rsc.org/materials

PAPER

Pyridinic N doped graphene: synthesis, electronic structure, and electrocatalytic property†

Zhiqiang Luo,[ab] Sanhua Lim,[b] Zhiqun Tian,[b] Jingzhi Shang,[a] Linfei Lai,[ab] Brian MacDonald,[c] Chao Fu,[c] Zexiang Shen,[a] Ting Yu*[ad] and Jianyi Lin*[b]

Received 25th February 2011, Accepted 24th March 2011
DOI: 10.1039/c1jm10845j

Different C–N bonding configurations in nitrogen (N) doped carbon materials have different electronic structures. Carbon materials doped with only one kind of C–N bonding configuration are an excellent platform for studying doping effects on the electronic structure and physical/chemical properties. Here we report synthesis of single layer graphene doped with pure pyridinic N by thermal chemical vapour deposition of hydrogen and ethylene on Cu foils in the presence of ammonia. By adjusting the flow rate of ammonia, the atomic ratio of N and C can be modulated from 0 to 16%. The domain like distribution of N incorporated in graphene was revealed by the imaging of Raman spectroscopy and time-of-flight secondary ion mass spectrometry. The ultraviolet photoemission spectroscopy investigation demonstrated that the pyridinic N efficiently changed the valence band structure of graphene, including the raising of density of π states near the Fermi level and the reduction of work function. Such pyridinic N doping in carbon materials was generally considered to be responsible for their oxygen reduction reaction (ORR) activity. The 2e reduction mechanism of ORR on our CN_x graphene revealed by rotating disk electrode voltammetry indicated that the pyridinic N may not be an effective promoter for ORR activity of carbon materials as previously expected.

Introduction

The great interest in graphene, a two-dimensional crystal made of carbon atoms arranged in a honeycomb lattice, is mainly due to its intriguing physical, chemical and mechanical properties originating from its novel electronic band structures.[1,2] The deliberate introduction of dopants into graphene could offer a possible route to tailor its electronic band structure, which is of great technological importance for its potential applications in nanoelectronics, nanophotonics, sensor devices, and green energy technology.[2–5] As the neighbors of carbon (C) in the periodic table, boron (B) and nitrogen (N) are the mostly studied dopants for carbon materials,[6,7] which would provide p- and n-doping, respectively. Theoretical studies show that the B/N substitutional doping can modulate the band structure of graphene without impeding its good conducting behavior.[8] Recently, Ci *et al.* reported the synthesis of two dimensional BCN single layer sheet containing hybridized bonds involving elements B, N and C over wide compositional ranges, and their novel electronic and optical properties were distinct from those of pure graphene and BN graphene.[9]

In this work, we demonstrate the synthesis of N-doped single layer graphene (CN_x graphene) with N percentage up to 16% by thermal chemical vapour deposition (CVD) of hydrogen (H_2) and ethylene (C_2H_4) on Cu foils in the presence of ammonia (NH_3). The chemical components and electronic structures of the as synthesized CN_x graphene were characterized by Raman spectroscopy, time-of-flight secondary ion mass spectrometry (TOF-SIMS), X-ray photoelectron spectroscopy (XPS), and ultraviolet photoemission spectroscopy (UPS). The electronic structure characterization indicates the incorporated N is in pure pyridinic N–C bonding configuration. Since graphene layers doped by nearly pure graphitic N were previously synthesized by pyrolysis of methane (CH_4) and NH_3 on Cu foils, controllable N doping in graphene makes graphene an excellent platform for studying the doping effect of pure pyridinic/graphitic N on the

[a]Division of Physics and Applied Physics, School of Physical and Mathematical Sciences, Nanyang Technological University, Singapore 637371. E-mail: Yuting@ntu.edu.sg
[b]Applied Catalysis, Institute of Chemical and Engineering Sciences, Singapore 627833. E-mail: lin_jianyi@ices.a-star.edu.sg
[c]WinTech Nano-Technology Services Pte. Ltd, Singapore 117684
[d]Department of Physics, Faculty of Science, National University of Singapore, Singapore 117542

† Electronic supplementary information (ESI) available: Optical image of single layer graphene transferred onto a SiO_2/Si substrate, Raman spectra and imaging of CN_x graphene synthesized with the NH_3/He flow rate of 12 sccm (GN12), overlay imaging of CN- and C_2- mass spectra images, TOF-SIMS mass spectra in linear scale, calculation of electron transfer numbers in ORR, XPS survey scan of CN_x graphene synthesized with the NH_3/He flow rate of 6 sccm (GN6), and its N1s core-level spectrum in a wider range (390 eV–408 eV). See DOI: 10.1039/c1jm10845j

physical and chemical properties, such as electron and phonon transport properties, optical properties, and chemical activity.[10]

Experimental details

The single layer graphene was grown on 34 μm Cu foils (99.95% purity, Goodfellow, UK) by low pressure CVD using ethylene (C_2H_4) and hydrogen (H_2) as gas source. Such large scaled CVD synthesis of graphene on high purity Cu substrates has been well developed in several research groups by pyrolysis of methane (CH_4) and H_2.[11–13] The Cu foil was heated up and annealed at 900 °C for 30 min in the flowing 10 sccm H_2 at 1 Torr. The gas mixture of H_2 and C_2H_4 was then flowed at 4.6 Torr with a rate of 30 sccm and 10 sccm for 30 min, respectively. After the growth, the samples were cooled down to room temperature (~20 °C min^{-1}) with flowing H_2 under the pressure of 1 Torr. For the growth of CN_x-graphene, NH_3 diluted in He (NH_3/He, v/v 10%) with the flow rate of 3–12 sccm was introduced into the reactor during the graphene growth process without changing the flow rates of H_2 and C_2H_4.

With $(NH_4)_2S_2O_8$ (0.1 M) as Cu etchant, the graphene or CN_x graphene on Cu foils was transferred onto the Si wafer substrate with 285 nm SiO_2 cap layer for Raman spectroscopy and contrast spectroscopy characterizations. The large area transferred graphene on a SiO_2/Si substrate is demonstrated in Figure S1 in supporting information. The Raman and contrast spectroscopy were performed on a WITEC CRM200 Raman system using a 100x objective lens with a numerical aperture (NA) of 0.95. The excitation source for Raman spectroscopy was a 532 nm laser (2.33 eV) with a laser power below 1 mW to avoid laser-induced heating. The illumination source for the contrast spectroscopy was normal white light. For Raman imaging, the sample was placed on an X–Y piezo-stage and scanned under the illumination of laser light with a step size of 250 nm.

XPS and UPS studies of the graphene/CN_x graphene on Cu foils were performed using ESCALAB 250 (Thermo VG Scientific). For the XPS analysis, monochromatic Al Kα ($h\nu = 1486.6$ eV) excitation was employed. For the UPS analysis, a He lamp was used with 21.2 eV (He I) and 40.8 eV (He II) excitation energies. TOF-SIMS study of the CN_x graphene on Cu foils was performed on TOF-SIMS[5] (ION-TOF GmbH) using 50 KeV Bi_3^{++} as ion beam. The lateral resolution for SIMS imaging is 100 nm.

For electrochemical measurements, two layers of graphene/CN_x graphene were transferred onto the glassy carbon (GC) disk electrode (5 mm in diameter, Eco Chemie, Netherlands) through the layer by layer transfer method.[12] The electrodes were dried at 60 °C for 120 min. Oxygen reduction reaction (ORR) voltammograms were recorded using an Autolab potentiostat (Eco Chemie BV) with a three-electrode system in an oxygen saturated 0.1 M KOH (pH 13) electrolyte solution. The graphene/CN_x-graphene on the glassy carbon rotating disk electrode (RDE) was used as a working electrode, with the rotating rate varying from 250 rpm to 2000 rpm. An Ag/AgCl electrode was used as a reference electrode and Pt sheet was used as a counter electrode.

Results and discussion

Fig. 1a displays the Raman spectrum of the CVD grown graphene transferred onto a SiO_2/Si substrate. Two strong peaks characteristic of single layer graphene at ~1580 cm^{-1} and at ~2670 cm^{-1} have been respectively assigned to the G band, in-plane vibrational mode (E_{2g} phonon at the Brillouin zone center), and the 2D band, intervalley double resonance scattering of two TO phonons around the K-point of the Brillouin zone.[14,15] In addition to the characteristic G and 2D Raman peaks, the CVD grown graphene also shows a weak Raman peak at 1340 cm^{-1}, which has been assigned to D band activated by defects *via* an intervalley double-resonance Raman process.[15,16] Commonly the intensity ratio of D band to G band (I_D/I_G) has been used to evaluate the defect density in graphene.[16–19] The small amount of defects in graphene should be formed during the CVD process. The single layer feature of CVD grown graphene was also confirmed by contrast spectrum.[20] As shown in the inset of Fig. 1a, the contrast peak value of the graphene transferred onto 285 nm SiO_2/Si is 0.1, close to the calculation value of that for single layer graphene.[20,21]

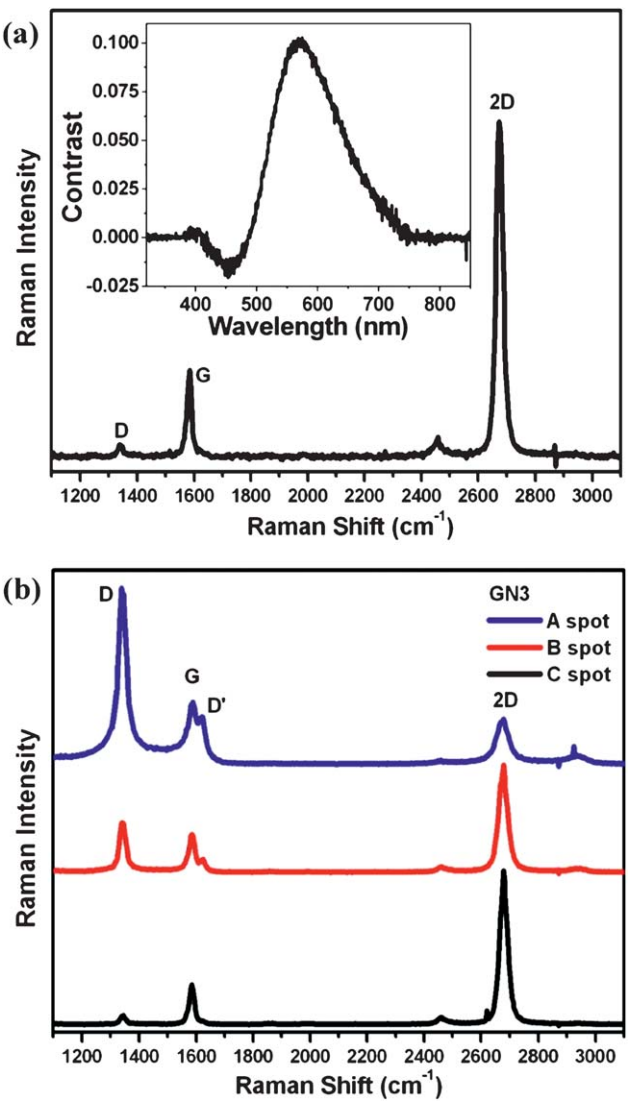

Fig. 1 (a) Raman spectrum of the CVD graphene; the inset shows the contrast spectra of the CVD graphene on 300 nm SiO_2/Si substrate. (b) Raman spectra of the CN_x graphene synthesized with the NH_3/He flow rate of 3 sccm (GN3).

The N-doping greatly enhances the defect density in the CN_x graphene as shown by the strong D band in Fig. 1b. The distribution of defects (incorporated N) in the N-doped graphene is inhomogeneous. Fig. 2a and 2b respectively are the D and 2D band Raman imaging of the CN_x graphene synthesized with 3 sccm NH_3/He flow rate (GN3). Both the D and 2D band images are not uniformly distributed but compensating to each other in terms of bright/dark areas, indicating that the defects exist in domains. The A and B spots in the bright D imaging area in Fig. 2a show strong D and D′ (activated by defects *via* an intravalley double-resonance process) bands in Fig. 1b, while they are associated with low 2D band intensity (black areas in Fig. 2b), indicating high defect density, *i.e.* N rich area. The B area is located bordering the domains, with much lower different defect density than that in the center of domains. The C type area is dominant in this sample, with nearly the same Raman spectrum as the pristine CVD graphene, indicating no N incorporated in such areas.

When the NH_3/He flow rate is increased, the Raman spectra corresponding to the A, B, C areas keep nearly unchanged (see Figure S3 in supporting information), but the domain size of the A area, *i.e.* N rich area, increases obviously, as shown in the D and 2D band Raman imaging (Fig. 2c and 2d) of the CN_x graphene synthesized with 6 sccm NH_3/He flow rate (GN6). The continuous and single layered graphitic structure in the N-rich area is evidenced by featureless G band Raman imaging (see Figure S2 in supporting information). The distribution of N in graphene was further investigated by time-of-flight secondary ion mass spectrometry (TOF-SIMS) imaging. With the ion beam bombardment on the CN_x graphene sample surface, characteristic mass fragments from the C and CN fractions, including C^-, C_2^-, C_3^-, C_4^-, and CN^-, are demonstrated on the negative ion spectra (see supporting information). The CN^- peak with strong intensity indicates the incorporation of N in the graphene lattice. Similar to the Raman imaging, the chemical imaging generated from the CN^- and the dominant C fraction (C_2^-), as shown in Fig. 3, clearly shows the domain distribution of the N in graphene sheet.

To determine the N/C atomic ratio and the bonding configurations of incorporated N in the CN_x graphene, XPS was performed on the CN_x graphene samples. Fig. 4a and 4b are the C1s and N1s core-level spectra of the CN_x graphene synthesized with 6 sccm NH_3/He flow rate (GN6). A survey of XPS and N1s core-level spectra in a wider range (390 eV–408 eV) is shown in supporting information (see Figure S6). The C1s peak can be fitted with two components: the main peak at binding energy (BE) of 284.4 eV (C1) is assigned to sp^2 hybridized C atoms in graphene while another peak located at 285.5 eV (C2) should be assigned to sp^2 C atoms bonded with N.[10,22] The C–N peak shifts to 285 eV at lower N doping level as indicated in Table 1 (spectra not shown here). The binding energy of N1s located at 399.3 eV may originate from sp states of N (–C≡N, carbonitrile groups) or from sp^2 hybridized N atoms with two sp^2 hybridized C neighbors (C=N–C, pyridinic N) with adjacent carbon vacancies.[7,23–26] Since the C1s corresponding to carbonitrile groups, which is around 286.5 eV,[27,28] was not observed, we can surely assign the 399.3 eV peak to pyridinic N. The N1s spectrum is very sharp (full width at half-maximum, 0.75 eV), which can only be fitted with one peak component as shown in Fig. 3b, indicating the pure pyridinic N bonding configuration formed in our CN_x graphene samples, since the other two possible N bonding configurations in graphene, pyrrolic (N incorporated in five-membered heterocyclic ring) and graphitic (or quaternary, sp^2 hybridized N bonded with three sp^2 hybridized C neighbors) N would have greater binding energies between 400.5 and 401.3 eV.[7,23,25] The N/C atomic ratios in CN_x graphene synthesized with different ammonia flow rate are shown in Table 1. The N/C atomic ratio reaches its maximum (16%) with the ammonia flow rate of 6 sccm, and then decreases with the increasing of ammonia flow rate. Such a decrease of N/C atomic ratio with the increasing of ammonia flow rate was previously reported in synthesis of N doped carbon nanotubes, which may be caused by

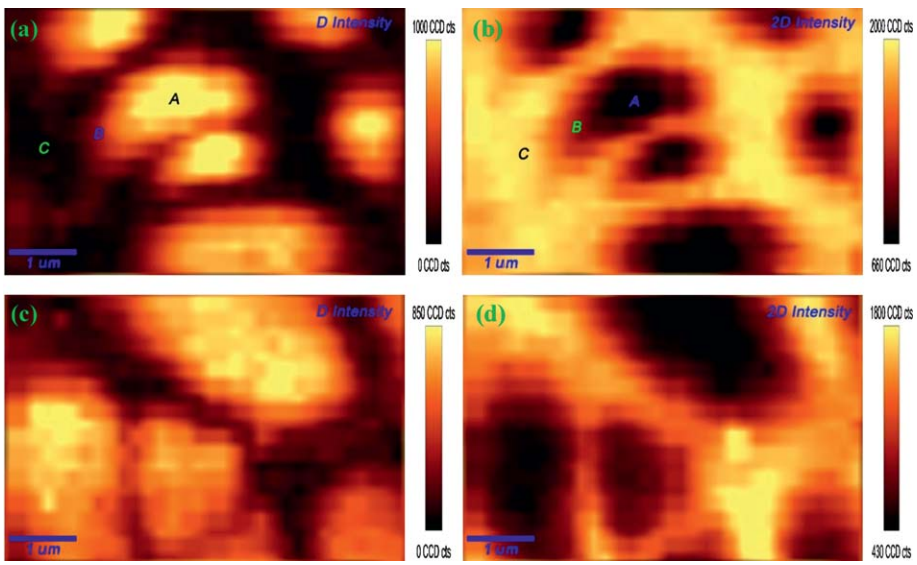

Fig. 2 (a) D and (b) 2D band intensity Raman imaging of CN_x graphene synthesized with the NH_3/He flow rate of 3 sccm (GN3); (c) D and (d) 2D band intensity Raman imaging of CN_x graphene synthesized with the NH_3/He flow rate of 6 sccm (GN6). The imaging area is 6 μm × 4 μm.

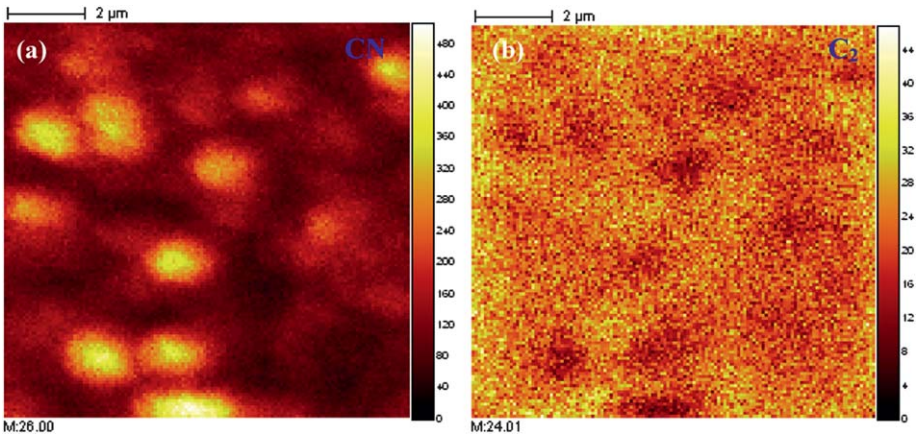

Fig. 3 2D TOF-SIMS images of CN_x graphene synthesized with the NH_3/He flow rate of 6 sccm (GN6) generated from the (a) CN^- intensity and (b) C_2^- intensity. The imaging area is 10 μm × 10 μm.

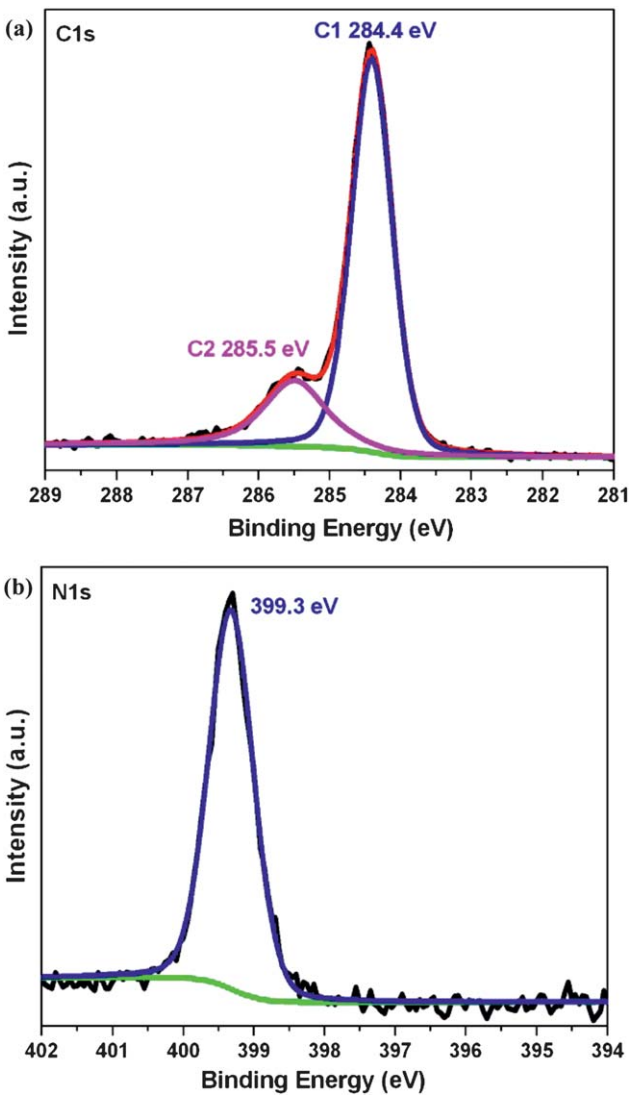

Fig. 4 (a) C1s and (b) N1s core-level X-ray photoelectron spectra of CN_x graphene synthesized with the NH_3/He flow rate of 6 sccm (GN6).

Table 1 Variation of N/C atomic ratio, C1s/N1s binding energy and C1s/N1s peak width (FWHM) of CN_x graphene synthesized with different NH_3/He flow rates

NH_3/He Flow (sccm)	0	3	6	9	12
N/C ratio (%)	0	1.6	16	6	2.2
C1s (C1) BE (eV)	284.4	284.35	284.4	284.35	284.35
C1s (C1) FWHM (eV)	0.7	0.7	0.7	0.7	0.7
C1s (C2) BE (eV)	—	285	285.5	285.2	285.1
C1s (C2) FWHM (eV)	—	1.2	1	1.25	1.3
N1s BE (eV)	—	399.35	399.3	399.35	399.4
N1s FWHM (eV)	—	0.8	0.75	0.75	0.75

the instability of chemisorbed N on C at high N radical concentation.[29,30] Since the above measured N/C atomic ratios are an average value over a large probed area (spot size of the X-ray is around 500 μm), the N/C atomic ratio in the N rich area (A area in Fig. 2a) should be even larger.

The valence-band (VB) electronic structure of the CN_x graphene was probed with UPS. Fig. 5a and 5b show the He II and He I valence band spectra respectively for the CN_x graphene synthesized with different N/C atomic ratios. The pristine CVD graphene (CVD-G, Fig. 4a) shows five peaks, which are assigned to: (1) C 2p π between 0 and 4 eV; (2) the crossing of C 2p π and C 2p σ bands around 5.9 eV; (3) C 2p σ at 7.9 eV; (4) C 2s–2p hybridized state at 10.6 eV; and (5) C 2s σ band at ~13.3 eV.[31] After N incorporation with 3 sccm NH_3/He flow (G900-N3), the He II spectrum remains the same as that of pristine CVD graphene. Upon N incorporation with increasing NH_3/He flow rate (GN6 and GN9), two distinct features appear in the He II spectrum, at approximately 4.9 and 7.2 eV, which appear to originate from N lone pair state (a pair of electrons strongly localized on the N atom) and delocalized C–N 2pπ state (C–N π) of the pyridinic N, respectively.[26,27,32] By peak analysis, it is noted that the intensity ratio of the C–N π component and N lone pair component is around 0.9 for the GN6 and GN9 samples, in good agreement with the ratio of two C–N p bonding over two lone-pair electrons in pyridinic configuration. The (C–N π/N lone pair) ratio increases to 1.2 for the GN12 samples, indicating the enhancement of C–N π component in the CN_x graphene

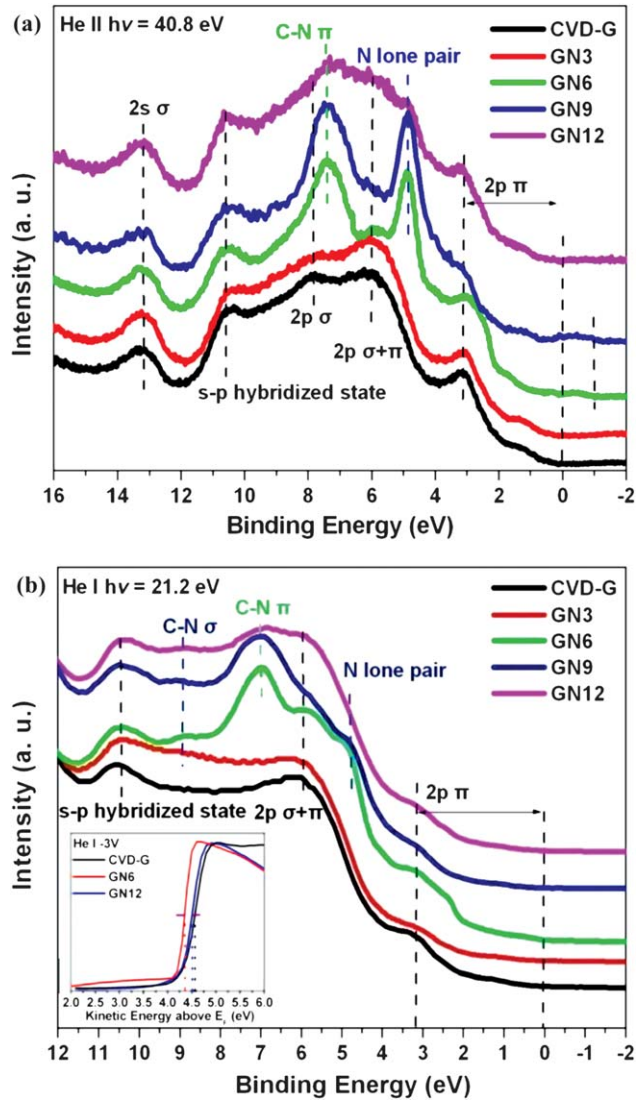

Fig. 5 Relative variation of (a) He II and (b) He I UPS valence band spectra of CN_x graphene synthesized with different NH_3/He flow rates. The inset of (b) shows low-energy cutoff of the valence band (measured with He I radiation) of graphene and CN_x graphene as a function of kinetic energy relative to the Fermi level. These spectra have been measured with a sample bias of −3 V.

synthesized with high NH_3/He flow rate. The N-doping induced features are also observable in He I spectra. Furthermore another extra feature located at 9 eV can be observed in the He I spectrum for all CN_x graphene samples, which should be assigned to the C–N σ bonds.[32]

The N doping may result in the enhancement of state density near the Fermi level. In both He II and He I spectra, the delocalized 2pπ states of GN6 get more pronounced and there appears an additional state at 2.3 eV as a shoulder of the 2pπ peak, whereas the delocalized C 2pπ states of GN3, GN9 and GN12 show significant depression. Each N atom has five 2p valence electrons *vs.* four per C atom. The substitution of electron-rich N into the C network in the form of graphitic N would contribute with two electrons to the π electron system as compared to one π electron per carbon atom. The extra electron may enter the π* state, giving a "π doping" effect.[7] The pyridinic N atom is bonded to two neighboring C with forming of C vacancies in the graphene sheet. The two electrons contribute to the localized N lone pair state, and the pyridinic N only exhibits a weak doping effect if next to a vacancy.[7] The pyridinic N incorporation in the C network would enhance C–N 2pπ states while depressing the C–C 2pπ electron state density, as observed in samples GN9 and GN12. The observation of enhanced C–C 2pπ states in GN6 sample should be attributed to the presence of a shoulder state at 2.3 eV, which may originate from the 2pπ states of the sp^2 C clusters separated by N in the domains with high N/C ratio,[7] in analogy to the 2pπ states of C dimer (>C═C<) located at about 2 eV.[33] At a high N/C ratio, the doping effect induced apparent change in density of π states near the Fermi level as shown in Fig. 5a, where the Fermi level (E_F) of pristine graphene is located at BE = 0 eV, while for CN_x graphene with high N/C atomic ratio (GN6 and GN9), the raising of the state density at BE = 0 eV is observable. This is consistent with the results of work function measurements by using biased He I UPS. As shown in the inset of Fig. 4b, the secondary electron tail threshold of the GN6 sample is shifted by 0.2 eV towards lower kinetic energy in comparison to that of pristine CVD graphene (CVD-G), indicative of a reduction in work function by 0.2 eV. Previously, a larger reduction of work function by 0.5 eV was found in our N doped carbon nanotube (CN_xNT, x = 12 at.%) with a high fraction of graphitic N.[22]

Both XPS and UPS characterizations confirmed the pure pyridinic N–C bonding configuration in our CN_x graphene. N doped graphene layers with nearly pure graphitic C–N bonding were previously synthesized by Wei *et al.*[10] Note that pure pyridinic/graphitic N have never been reported during N doping of other carbon materials, such as carbon nanotubes, although N doping in carbon nanomaterials has been studied for decades during intensive study of the synthesis technique.[6,7] Different C–N bonding configurations in N doped carbon materials have different electronic structures and therefore different physical and chemical properties.[7] The N doped graphene with only one kind of C–N bonding configuration is an excellent platform for studying the doping effect on the physical and chemical properties, such as electron and phonon transport properties, optical properties, and chemical activity. Recently, N-doped graphene layers were demonstrated as a promising Pt-free catalyst for oxygen reduction reaction (ORR) with high activity and high durability, which can be applied as nonprecious electrodes in polymer electrolyte membrane fuel cells and electrochemical biosensors.[34,35] The novel catalytic properties of N doped carbon materials have been attributed to electronic structure changes caused by the N incorporation into the graphitic structure.[36] However, which kind of C–N bonding configurations should be responsible for the enhanced catalytic activity of N-doped carbon materials is under discussion.[37–40] Generally, either pyridinic or pyrrolic type N is considered to be responsible for the ORR activity of carbon nanostructures.[37] Since the N doped carbon materials reported previously always contained several kinds of C–N bonding configurations, our CN_x-graphene incorporated with pure pyridinic N would offer a good opportunity to check the ORR activity of the N–C bonding in pyridinic configuration.

Fig. 6a displays the ORR polarization curves on CN_x graphene with different N/C atomic ratios. For comparison, the

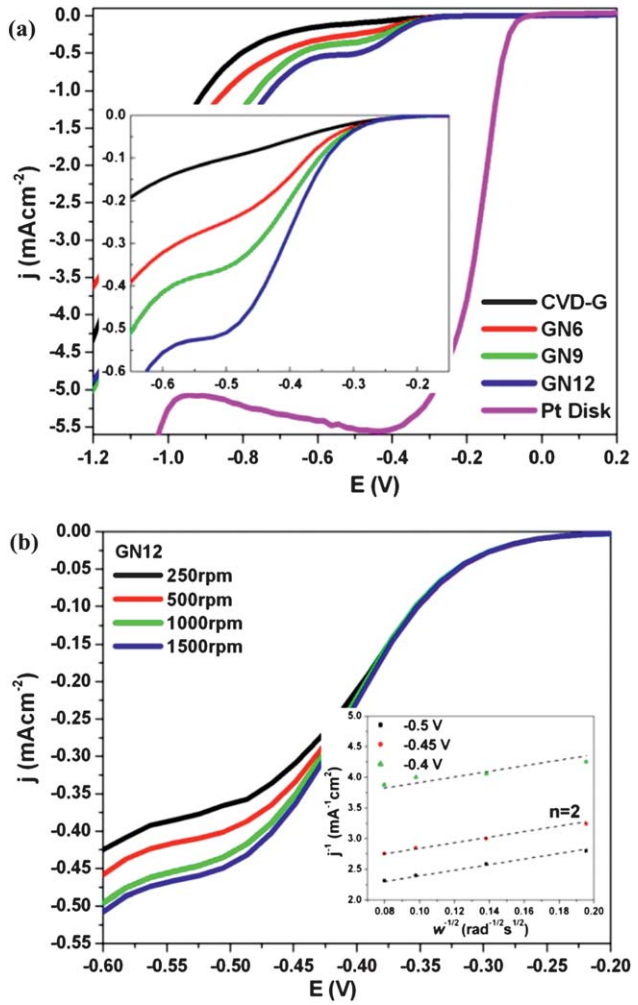

Fig. 6 (a) RDE voltammetry curves for the ORR in O_2 saturated 0.1 M KOH at the CVD graphene electrode, CN_x graphene electrodes and Pt disk electrode; the inset shows the enlargement of the curves in the range of −0.15 to −0.65 V. Electrode rotating rate: 2000 rpm. Scan rate: 0.01 V s^{-1}. (b) RDE voltammetry curves for the ORR at the CN_x graphene (GN12) electrode with various rotation speeds; the inset shows the Koutecky–Levich plots for ORR on CN_x graphene (GN12) electrode.

curves on the pristine graphene (CVD-G) and the Pt disk electrode (Eco Chemie, Netherlands) are also shown. All the graphene samples, with or without N incorporation, show a poor ORR activity with high onset potential (−0.3 V) as compared to Pt disk. Nevertheless the CN_x graphene exhibits somehow enhanced ORR activity with faster increase of current density (j) above the potential of −0.6 V, in the order of GN12 > GN9 > GN6 > CVD-G. As shown in the inset of Fig. 6a, a steeper slope demonstrates better ORR activity. Note that the ORR activity of CN_x-graphene is not proportional to the total amount of the incorporated N. Despite having lower N content, GN12 electrode (2.2 at.%) shows better ORR activity than that of GN6 electrode (16 at.%). Recent DFT calculation shows that the incorporated N itself is not the active site for ORR, but the C atom adjoining a N atom has a reduced energy barrier to ORR.[41] Doping of electronegative N atoms reduces the electron density of C atoms that bond with N atoms and polarizes the C atoms into C(δ+), making it easy for adsorption of the O_2 (O–O) molecule, which is the first step in the ORR process.[41,42] Subsequent electron transfer between C(δ+) and O–O will result in formation of radical anions.[41,42] However, since O_2 molecule has high density of O lone pair electrons, the polarized pyridinic N(δ−), with high density of N lone pair electrons, may have a higher energy barrier for the O_2 activation caused by the high repulsion interaction with the O_2 approaching the adjoining C(δ+) atoms.[42] Therefore, the balance between the C(δ+)–O_2 and N(δ−)–O_2 interactions would cause an optimized N concentration for the desired O_2 activation.

Fig. 6b shows the RDE voltammograms of oxygen reduction on GN12 electrode with various rotation speeds (w). Using the Koutechy–Levich equation,[43] the electron transfer numbers were calculated with the plotting of j^{-1} *vs.* $w^{-1/2}$ (see supporting information), as shown in the inset of Fig. 6b. At the potential ranging from −0.4 to −0.6 V, the electron transfer numbers calculated are close to 2, suggesting the 2 electron (2e) reduction pathway in the incomplete O_2 reduction to hydrogen peroxide (H_2O_2). At more negative potentials (<−0.6 V), the H_2O_2 was further reduced to H_2O.[43] Different from the excellent ORR activity with the 4 electron (4e) reduction pathway from O_2 directly to H_2O on the N doped carbon nanotubes and graphene layers reported by other research groups,[34,36] the ORR activity of our CN_x graphene with 2e reduction mechanism is much lower. In their samples, both the pyridinic N and the pyrrolic N were incorporated, with binding energies located at 398.3 eV and 400.5 eV, respectively.[34] According to intensive X-ray absorption analysis of various N incorporated in carbon nanostructures, Niwa *et al.* found that the samples with a relatively larger amount of graphitic N (X-ray absorption peak at 401.5 eV) exhibit a higher ORR activity than those with a relatively larger amount of pyridinic N (X-ray absorption peak at 399.1 eV).[39] Recently, Nagaiah *et al.* also reported that in carbon nanotubes doped by various N, graphitic N played a more important role in the enhanced ORR activity in alkaline solution than the pyridinic N.[40] It seems that our result is a more direct support for the observation that C–N bonding in pyridinic configuration may not be an effective promoter for ORR activity. The above-mentioned repulsion interaction between dense lone pair electrons in both pyridinic N(δ−) and O_2 may be partially responsible for the observed ORR performance of pyridinic N. There are no such dense lone pair electrons in the graphitic N.[7] It also should be pointed out that different ORR performance in the literature may partially result from different binding energies of pyridinic N in different samples, because the reported binding energies of pyridinic N varied in a wide range of 398.3–399.3 eV.[25,28,34,35] Further work in comparing the ORR activity of the graphene samples with pure pyridinic/pyrrolic/graphitic N configurations is needed to clarify the origin of novel ORR activity in N-doped carbon materials.[10]

Conclusions

Nitrogen-doped single layer graphene (CN_x graphene) incorporated with N percentage up to16% was synthesized by thermal chemical vapour deposition of hydrogen and ethylene on Cu foils in the presence of ammonia. The Raman spectroscopy and TOF-SIMS images show that the incorporated N in graphene is in

domain like distribution. The pure pyridinic N–C bonding configuration in CN_x graphene was confirmed by the XPS and UPS investigation. Moreover, the UPS investigation demonstrated that pyridinic N efficiently changed the valence band structure of graphene, including the raising of density of π states near the Fermi level and the reduction of work function. The 2e reduction mechanism of the pyridinic N in ORR found in our experiments suggests that the pyridinic N may not be an effective promoter as previously expected.

Acknowledgements

Authors acknowledge the support by the Singapore National Research Foundation under NRF RF Award No. NRF-RF2010-07 and MOE Tier 2 MOE2009-T2-1-037.

References

1 A. H. Castro Neto, F. Guinea, N. M. R. Peres, K. S. Novoselov and A. K. Geim, *Rev. Mod. Phys.*, 2009, **81**, 109–162.
2 Y. H. Wu, T. Yu and Z. X. Shen, *J. Appl. Phys.*, 2010, **108**, 071301.
3 F. Schwierz, *Nat. Nanotechnol.*, 2010, **5**, 487–496.
4 N. Papasimakis, Z. Q. Luo, Z. X. Shen, F. D. Angelis, E. D. Fabrizio, A. E. Nikolaenko and N. I. Zheludev, *Opt. Express*, 2010, **18**, 8353–8359.
5 M. D. Stoller, S. Park, Y. Zhu, J. An and R. S. Ruoff, *Nano Lett.*, 2008, **8**, 3498–3502.
6 A. Jorio, G. Dresselhaus, M. S. Dresselhaus, (ed.), *Carbon Nanotubes: Advanced Topics in the Synthesis, Structure, Properties and Applications* (Berlin: Springer), 2008, pp. 531–566.
7 V. A. Basiuk, E. V. Basiuk, (ed.), *Chemistry of Carbon Nanotubes* (American Scientific Publishers), 2007, pp. 113–141.
8 A. Lherbier, X. Blase, Y. M. Niquet, F. Triozon and S. Roche, *Phys. Rev. Lett.*, 2008, **101**, 036808.
9 L. Ci, L. Song, C. Jin, D. Jariwala, D. Wu, Y. Li, A. Srivastava, Z. F. Wang, K. Storr, L. Balicas, F. Liu and P. M. Ajayan, *Nat. Mater.*, 2010, **9**, 430–435.
10 D. Wei, Y. Liu, Y. Wang, H. Zhang, L. Huang and G. Yu, *Nano Lett.*, 2009, **9**, 1752–1758.
11 X. Li, W. Cai, J. An, S. Kim, J. Nah, D. Yang, R. Piner, A. Velamakanni, I. Jung, E. Tutuc, S. K. Banerjee, L. Colombo and R. S. Ruoff, *Science*, 2009, **324**, 1312–1314.
12 X. Li, Y. Zhu, W. Cai, M. Borysiak, B. Han, D. Chen, R. D. Piner, L. Colombo and R. S. Ruoff, *Nano Lett.*, 2009, **9**, 4359–4363.
13 Z. Q. Luo, T. Yu, J. Z. Shang, Y. Y. Wang, S. H. Lim, L. Liu, G. G. Gurzadyan, Z. X. Shen and J. Y. Lin, *Adv. Funct. Mater.*, 2011, **21**, 911–917.
14 Z. H. Ni, Y. Y. Wang, T. Yu and Z. X. Shen, *Nano Res.*, 2008, **1**, 273–291.
15 A. C. Ferrari, *Solid State Commun.*, 2007, **143**, 47–57.
16 M. A. Pimenta, G. Dresselhaus, M. S. Dresselhaus, L. G. Cancado, A. Jorioa and R. Saito, *Phys. Chem. Chem. Phys.*, 2007, **9**, 1276–1291.
17 Z. Q. Luo, T. Yu, K. J. Kim, Z. H. Ni, Y. M. You, S. H. Lim, Z. X. Shen, S. Z. Wang and J. Y. Lin, *ACS Nano*, 2009, **3**, 1781–1788.
18 Z. Q. Luo, J. Z. Shang, S. H. Lim, D. H. Li, Q. H. Xiong, Z. X. Shen, J. Y. Lin and T. Yu, *Appl. Phys. Lett.*, 2010, **97**, 233111.
19 Z. Q. Luo, T. Yu, Z. H. Ni, S. H. Lim, H. L. Hu, J. Z. Shang, L. Liu, Z. X. Shen and J. Y. Lin, *J. Phys. Chem. C*, 2011, **115**, 1422–1427.
20 Z. H. Ni, H. M. Wang, J. Kasim, H. M. Fan, T. Yu, Y. H. Wu, Y. P. Feng and Z. X. Shen, *Nano Lett.*, 2007, **7**, 2758–2763.
21 C. Casiraghi, A. Hartschuh, E. Lidorikis, H. Qian, H. Harutyunyan, T. Gokus, K. S. Novoselov and A. C. Ferrari, *Nano Lett.*, 2007, **7**, 2711–2717.
22 S. H. Lim, H. I. Elim, X. Y. Gao, A. T. S. Wee, W. Ji, J. Y. Lee and J. Y. Lin, *Phys. Rev. B: Condens. Matter Mater. Phys.*, 2006, **73**, 045402.
23 E. N. Nxumalo and N. J. Coville, *Materials*, 2010, **3**, 2141–2171.
24 C. Quiros, J. Gomez-Garcia, F. J. Palomares, L. Soriano, E. Elizalde and J. M. Sanz, *Appl. Phys. Lett.*, 2000, **77**, 803–805.
25 W. J. Gammon, O. Kraftb, A. C. Reillya and B. C. Holloway, *Carbon*, 2003, **41**, 1917–1923.
26 S. Souto, M. Pickholz, M. C. dos Santos and F. Alvarez, *Phys. Rev. B: Condens. Matter*, 1998, **57**, 2536–2540.
27 N. Hellgren, J. Guo, Y. Luo, C. Sathe, A. Agui, S. Kashtanov, J. Nordgren, H. Agren and J. Sundgren, *Thin Solid Films*, 2005, **471**, 19–34.
28 J. M. Ripalda, I. Montero and L. Galan, *Diamond Relat. Mater.*, 1998, **7**, 402–406.
29 J. Liu, S. Webster and D. L. Carroll, *J. Phys. Chem. B*, 2005, **109**, 15769–15774.
30 S. H. Lim, R. J. Li and J. Y. Lin, *Phys. Rev. B: Condens. Matter Mater. Phys.*, 2007, **76**, 195406.
31 A. Bianconi, S. B. M. Hagström and R. Z. Bachrach, *Phys. Rev. B: Solid State*, 1977, **16**, 5543–5548.
32 S. Bhattacharyya, C. Vallee, C. Cardinaud and G. Turban, *J. Appl. Phys.*, 2000, **87**, 7524–7532.
33 R. Graupner, M. Hollering, A. Ziegler, J. Ristein, L. Ley and A. Stampfl, *Phys. Rev. B: Condens. Matter*, 1997, **55**, 10841–10847.
34 L. Qu, Y. Liu, J. B. Baek and L. Dai, *ACS Nano*, 2010, **4**, 1321–1326.
35 Y. Wang, Y. Shao, D. W. Matson, J. Li and Y. Lin, Nitrogen-doped graphene and its application in electrochemical biosensing, *ACS Nano*, 2010, **4**, 1790–1798.
36 K. Gong, F. Du, Z. Xia, M. Durstock and L. Dai, *Science*, 2009, **323**, 760–764.
37 Y. Shao, J. Sui, G. Yin and Y. Gao, *Appl. Catal., B*, 2008, **79**, 89–99.
38 C. V. Rao, C. R. Cabrera and Y. Ishikawa, *J. Phys. Chem. Lett.*, 2010, **1**, 2622–2627.
39 H. Niwa, K. Horiba, Y. Harada, M. Oshima, T. Ikeda, K. Terakura, J. Ozaki and S. Miyata, *J. Power Sources*, 2009, **187**, 93–97.
40 T. C. Nagaiah, S. Kundu, M. Bron, M. Muhler and W. Schuhmann, *Electrochem. Commun.*, 2010, **12**, 338–341.
41 R. A. Sidik, A. B. Anderson, N. P. Subramanian, S. P. Kumaraguru and B. N. Popov, *J. Phys. Chem. B*, 2006, **110**, 1787–1793.
42 Y. Okamoto, *Appl. Surf. Sci.*, 2009, **256**, 335–341.
43 J. Zhang, (ed.), *PEM Fuel Cell Electrocatalysts and Catalyst Layers* (Springer), 2008, pp. 89–109.

